Diamond & Related Materials 17 (2008) 1927–1932

Contents lists available at ScienceDirect

Diamond & Related Materials

journal homepage: www.elsevier.com/locate/diamond

Evolution of compressive stress and electrical conductivity of tetrahedral amorphous carbon films with phosphorus incorporation

Aiping Liu *, Huaping Wu, Jiaqi Zhu, Jiecai Han, Li Niu

Center for Composite Materials, Harbin Institute of Technology, P.O. Box 3010, Yikuang Street 2, Harbin 150080, China

ARTICLE INFO

Article history:
Received 5 April 2007
Received in revised form 7 April 2008
Accepted 15 April 2008
Available online 20 April 2008

PACS:
81.15.Ef
78.66.Jg
62.40.+i
72.20.-i

Keywords:
Phosphorus incorporated tetrahedral amorphous carbon
Microstructure
Internal stress
Electrical conductivity

ABSTRACT

Successful modification of stress and conductivity for tetrahedral amorphous carbon (ta-C) films is realized by phosphorus incorporation via filtered cathodic vacuum arc technique with PH_3 as the impurity source. By establishing the structure as a function of phosphorus content, it is found that phosphorus fraction in phosphorus incorporated ta-C (ta-C:P) films increases with varying levels of PH_3 from 3 to 30 sccm, and that all samples retain their amorphous structures without remarkable changes, just exhibiting the clustering of sp^2 sites and the evolution of structural ordering. Furthermore, the addition of phosphorus causes the compressive stress relaxation in terms of the rearrangement in atomic bonding structures. The increased number of localized electronic π and π* states as hopping sites after phosphorus incorporation results in several orders of magnitude increase in the conductivity, and the films represent the hopping conduction in band tail states in the temperature range of 293–463 K. However, more H induced by excessive PH_3 may saturate some defects and compensate the hopping sites, leading to a slight drop in the conductivity. The nature of ta-C:P films as n-type semiconductors is proved from the features of rectifying current–voltage cures.

1. Introduction

Recently great attention has been given to amorphous carbon (a-C) or tetrahedral amorphous carbon (ta-C) films with respect to their potential applications in mechanical and electronic devices. However, the intrinsic compressive stress of the film with high sp^3 phases causes film delamination from the substrates if the film is grown beyond a critical thickness [1]. When considering the better use of ta-C films as semiconductor materials, the controlled variation of intrinsic stress and electrical conductivity through annealing and doping is of primary importance. It is shown that thermal annealing can release the stress, accompanied by subtle structural changes from as-grown films [2,3] and pronounced decrease in the resistivity [3]. However, the annealing method is limited by substrate materials owing to the difference in the expansion coefficients between the film and the substrate at a particular temperature [4]. Another solution to reduce the intrinsic stress of films is to introduce foreign impurities into the carbon network. In previous reports, various metallic and nonmetallic elements were attempted to decompress the constrained structures. For example, Tay et al. prepared Ti- and Al-containing a-C films and realized the relaxation of stress for the films [5]. Monteiro et al. [6] and Wang et al. [7] reported the stress relief of a-C films by incorporating a small percentage of W to the films. However, they paid no attention to the promotion of electrical behaviors. In the case of nonmetal addition, most studies concentrated on boron [8,9], nitrogen [10,11] and silicon elements [12]. These elements were confirmed to successfully decrease the compressive stress of films with proper development in the conductivity. When considering the active phosphorus in nature, it appears that phosphorus can also be introduced into a-C films to achieve n-type doping [13,14], and the resulted films show potential applications as photovoltaic solar cells [14,15], semiconductor field emitters [16] or biomedical coatings [17]. However, only limited work is devoted to the investigation about the structures, electrical characteristics and biocompatibility of phosphorus incorporated a-C (a-C:P) films [13–18]. An inconsistency of doping effect and graphitization of the bonding still exists in the role of impurity atoms in carbon films [13,14,18]. Therefore, a detailed study on the stress evolution and conduction mechanism related to the structural changes should be attempted.

In this paper, phosphorus incorporated ta-C (ta-C:P) films are prepared by filtered cathodic vacuum arc (FCVA) system with phosphine (PH_3) as the impurity source. The evolution of internal stress and conductivity with the variation of phosphorus contents in the films is described. The relaxation process of stress and the conduction mechanism are further

* Corresponding author. Tel./fax: +86 451 86417970.
E-mail address: liuaiping1979@gmail.com (A. Liu).

0925-9635/$ – see front matter © 2008 Elsevier B.V. All rights reserved.
doi:10.1016/j.diamond.2008.04.008

Table 1
Phosphorus content (P/(P+C)) obtained from XPS analysis and compressive stress determined from curvature measurements for ta-C and ta-C:P films prepared at different PH_3 flow rates

Sample	PH_3 flow rate (sccm)	Phosphorus content (at.%)	Compressive stress (GPa)
ta-C	0	0	7.8
ta-C:P_3	3	3.5	5.8
ta-C:P_{10}	10	6.8	3.5
ta-C:P_{20}	20	8.3	2.9
ta-C:P_{30}	30	16.8	0.2

The related error for all values is 5–7%.

discussed by investigating the correlation between structure, stress and electrical properties.

2. Experimental details

ta-C and ta-C:P films with thickness of 70–80 nm determined by a SE400 spectroscopic ellipsometry at a wavelength of 632.8 nm were deposited on p-type silicon wafer, insulating glass and quartz substrates by FCVA system described elsewhere [19]. In order to introduce the impurity, PH_3 (purity 99.9999%) gas was implanted into the vacuum chamber. The partial pressure of PH_3 varied from 2.4×10^{-5} to 2.7×10^{-4} Torr as PH_3 flow rate increased from 3 to 30 sccm. The samples were labeled as ta-C and ta-C:P_x (x=3, 10, 20 and 30, respectively) correspondingly.

Compositions of ta-C:P films were quantified from the total areas of X-ray photoelectron spectroscopy (XPS) signals corresponding to P 2p and C 1s core level spectra on a PHI ESCA 5700 spectrometer using Al K_α line (1486.6 eV) as the X-ray source. Because XPS was a subsurface technique, the subsurface atomic percentages of phosphorus (P/(P+C)) for all films were shown in Table 1. Notice that the films with phosphorus content over 5 at.% should probably be considered to be amorphous phosphorus carbide due to the high percentage of chemical bonds present between C and P atoms [20]. The microstructures of all samples were characterized by Raman measurement over the range from 1000 to 2000 cm^{-1} performed on a Jobin Yvon Labram HR 800 spectrometer with 458-nm Ar^+ laser as the excitation source. Infrared absorption spectra of the films were measured at room temperature on a Perkin Elmer spectrum DS Fourier Transform infrared (FTIR) spectrometer using a bare silicon substrate as the background reference. 64 scans over the region of 400–4000 cm^{-1} were averaged with a spectral resolution of 1 cm^{-1} in the FTIR experiments. The stress σ_R of the films was determined from the curvature measurements of silicon wafer before and after films deposition using a Dektak III profilometer and Stoney's equation [21]:

$$\sigma_R = \frac{E_S}{6(1-\nu_S)}\frac{t_S^2}{t_f}\left(\frac{1}{R_2}-\frac{1}{R_1}\right) \quad (1)$$

where E_S is Young's modulus of the substrate; υ_S is Poisson's ratio of the substrate; t_S and t_f are the thicknesses of the substrate and the films; R_1 and R_2 are the radii of curvature for the substrate before and after films deposition, respectively. UV/VIS/NIR absorption spectra of the films deposited on quartz substrates were recorded via a PerkinElmer Lambda 950 spectrometer ranging from 200 to 3000 nm with a spectral resolution of 1 nm. The optical band gap E_{04} was determined at the optical absorption coefficient equal to 10^4 cm^{-1} [22]. The resistances of all samples deposited on glass substrates were measured over the temperature range of 293–573 K by an electrometer (Keithley 617) or four-point probe. Gold strip electrodes were evaporated on the film surfaces at pressure below 10^{-5} Torr and stable contacts were provided by silver paste on the surfaces of gold electrodes before measurements. Au/ta-C:P/p-Si and Au/ta-C/p-Si structures were fabricated and current–voltage (I–V) measurements were performed using a semiconductor parameter analyzer (HP4156A) with a dc voltage source by evaporating gold dots of 2 mm in diameter and 10 nm in thickness on film surfaces and 100-nm thick Al films on Si substrate backs.

3. Results and discussion

3.1. Microstructures of ta-C:P films

Raman analysis is demanded to evaluate the structural arrangement of ta-C films after phosphorus introduction because of the sensitive and nondestructive features of Raman measurement for the characterization of bonding transformation in carbon materials. It can be seen from Raman spectra of ta-C and ta-C:P films deposited at different PH_3 flow rates (Fig. 1) that the lineshapes of all spectra are similar (except for an evident "peak shoulder" at about 1370 cm^{-1} for ta-C:P_{30} film) and indicate the amorphous structures of the films. In order to quantificationally analyze the spectra, we deconvolve the asymmetric bands with two Gaussian lines, namely D peak centered at 1370±5 cm^{-1} and G peak centered at 1557±10 cm^{-1}. It is well known that the G peak originates from zone centre phonons of E_{2g} symmetry for single crystal graphite and reflects the sp^2-bonded sites in both chains and rings. On the other hand, the D peak represents K-point phonons of A_{1g} symmetry for disordered graphite and suggests the sp^2 sites in aromatic rings. Notice that phosphorus introduction may change the polarizability of sp^2 clusters in ta-C film due to the difference of electronegativities between carbon and phosphorus. However, the modes of CP/CC are delocalized over both carbon and phosphorus sites because of the clustered sp^2 bonding induced by phosphorus. It is quite difficult to accurately distinguish the modes of CC and CP bonds considering the similarity of their vibrational frequencies. Assuming the similar variations of D and G peaks for ta-C:P films with low-P and high-P contents, the direct contributions of CP bonds to the spectra are neglected and the analysis method of G and D peaks for ta-C film is used to quantify the Raman spectra of ta-C:P films without considering heteropolar modes. Ferrari et al. also adopted analogous method to analyze the Raman spectra of amorphous carbon nitride with ~26 at.% N [23]. According to the viewpoint of Ferrari et al. [24], the intensity ratio of G and D peaks, $I_{(D)}/I_{(G)}$, is a crucial parameter to quantify the sp^3 content in carbon films. Our fitting results indicate that an increase of $I_{(D)}/I_{(G)}$ ratio from 0.31 to 0.61, a shift of G peak towards a lower wave number and a decrease in the full widths at half-maximum of G peak represent the clustering of sp^2

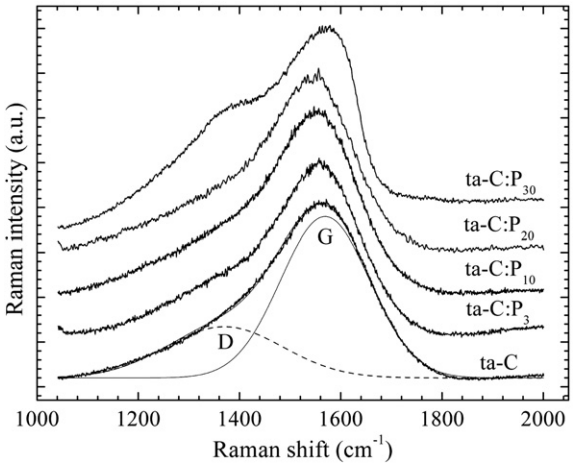

Fig. 1. Raman spectra of ta-C and ta-C:P films prepared at various PH_3 flow rates. Broad lines are the measurements; dash line and thin solid line are fitted D and G peaks, respectively.

groups, especially an evolution of aromatic sp^2 configuration [24] when phosphorus content in the films increases from 0 to 16.8 at.%.

Moreover, a significant photoluminescence (PL) background can be seen from the Raman spectrum of ta-C:P_{30} film. PL arises from the radiative recombination of electron-hole pairs trapped within the localized sp^2-bonded clusters in a sp^3-bonded amorphous matrix [25]. For ta-C:P films with lower phosphorus contents (P<9 at.%), the PL disappears or quenches. This phenomenon may be explained by the assumption that the carriers easily reach nonradiative centers by either hopping or tunneling and represent a nonradiative recombination. Following one of existing models [26], the PL intensity tends to increase with increasing H concentration. More H induced by excessive PH_3 possibly lengthens the localization radii of electron-hole pairs and leads to a loss in nonradiative recombination sites, which may make the hopping between clusters harder.

To further investigate the action of H in the carbon networks, FTIR measurements are carried out and the FTIR spectra of ta-C and ta-C:P films are demonstrated in Fig. 2. ta-C does not show significant IR signal. In contrast, ta-C:P films demonstrate IR activity since P increases the sp^2-C fraction (either by forming C=P or inducing C=C bonds) and the clustering of sp^2 phases. According to the standpoint of Ferrari et al. [23], high content sp^3-hybrided σ bonds of ta-C film have wider band gap and less polarity than sp^2-hybrided π bonds, and the remaining sp^2 sites are localized in isolated π bonds. Hence the enhancement in the IR activity after phosphorus implantation mainly originates from the large dynamic charge of the more delocalized π bonding in more sp^2-bonded networks. Based on the suggestion of Ferrari et al. [23], the IR spectra of ta-C:P films are considered to mostly consist of two different spectral regions: CP/CC modes and C–H bending modes at below 2000 cm^{-1}, and C–H stretching modes at 2800–3100 cm^{-1}. The band in the range of 1000–2000 cm^{-1} contains both CC skeleton modes at 1300–1400 cm^{-1} and 1550–1580 cm^{-1} and sp^3 $CH_{2,3}$ bending modes at 1375 cm^{-1} and 1460 cm^{-1} [23]. The C=P stretching specie may lie in the wave number range of 1300–1400 cm^{-1} similar to the CC modes [27]. The feature in the 1100–1300 cm^{-1} region is possibly due to the C–P stretching mode [27]. Considering the more sp^2 bonding and larger cluster sizes induced by phosphorus, these vibrational modes are delocalized and can not be accurately confined. Additionally, the 2330 cm^{-1} and 3600 cm^{-1} ranges may be attributed to C=O and H–O modes due to oxygen contamination on the sample surfaces and water vapor in the air.

Furthermore, the IR spectra are integrated after normalized to the thickness of each sample. It can be seen from Table 2 that there is an increment in the integrated area of 1000–2000 cm^{-1} band as phosphorus content increases, resulting from more sp^2-bonded network. The hydrogen atomic concentrations in the films can be approximately estimated by integrating the absorption peaks at around 3000 cm^{-1} [25]:

$$N_H = A \int \frac{\alpha(\omega)}{\omega} d\omega \quad (2)$$

where N_H is hydrogen atomic concentration; A is proportionality factor which is various for different peaks and different films; $\alpha(\omega)$ is absorption coefficient at frequency ω. It is clear that hydrogen content increases with PH_3 flow rate varying from 3 to 30 sccm. This is consistent with the increase of PL background in Raman spectra. The CH stretching band is further attributed to two main species, the sp^3-CH symmetrical/asymmetrical stretching at below 3000 cm^{-1} and sp^2-CH stretching at over 3000 cm^{-1} [28]. The area percentage of per part is calculated from the corresponding integral areas, as displayed in Table 2. Analysis results indicate that the percentage of sp^3-C bonded with H decreases first and increases later. This hints that excessive H may enhance the content of sp^3-C in the films when a large amount of PH_3 is introduced. Therefore, the main influence of H in ta-C:P films is to modify the carbon network by saturating isolated sp^3 dangling bonds and =C bonds as $=CH_x$ groups [25]. This possibly contributes to the decrease in the defects of clusters containing an odd number of sp^2 sites and the increase in PL efficiency of ta-C:P_{30} film.

Table 2
Integrated areas in the ranges of 1000–1800 and 2800–3100 cm^{-1}, and contents of sp^2 and sp^3 carbon atoms bonded with hydrogen for ta-C:P films prepared at different PH_3 flow rates

Sample	Integrated area (1000–1800 cm^{-1})	Integrated area (2800–3100 cm^{-1})	sp^3 C (%)	sp^2 C (%)
ta-C:P_3	40126.6	1000.7	86.4	13.6
ta-C:P_{10}	60708.1	1899.6	83.7	16.3
ta-C:P_{20}	64241.1	2353.9	84.1	15.9
ta-C:P_{30}	71423.2	4761.4	85.9	14.1

The related error for all values is less than 5%.

3.2. Compressive stress of ta-C:P films

Table 1 demonstrates the variation of intrinsic compressive stress of ta-C:P films with phosphorus content. The stress goes through a dramatic decrease when phosphorus fraction in the films goes up to 16.8 at.%. In order to better understand the relaxation process of stress, the stress versus $I_{(D)}/I_{(G)}$ ratio is plotted in Fig. 3. As seen from the figure, $I_{(D)}/I_{(G)}$ ratio exhibits a slight increase from 0.31 for ta-C to 0.38 for ta-C:P_{20}, accompanied with a pronounced fall in the compressive

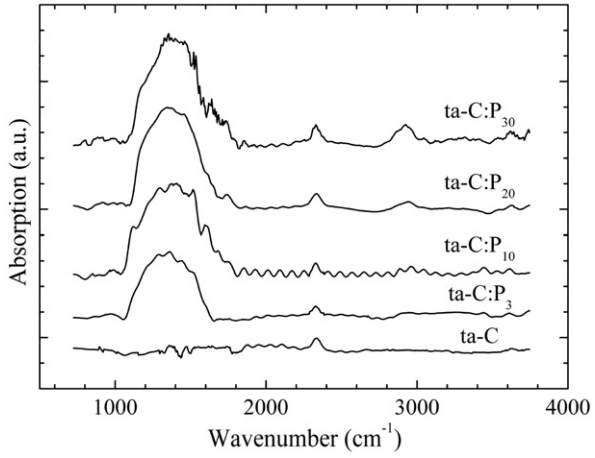

Fig. 2. Infrared absorption spectra of ta-C and ta-C:P films prepared at various PH_3 flow rates.

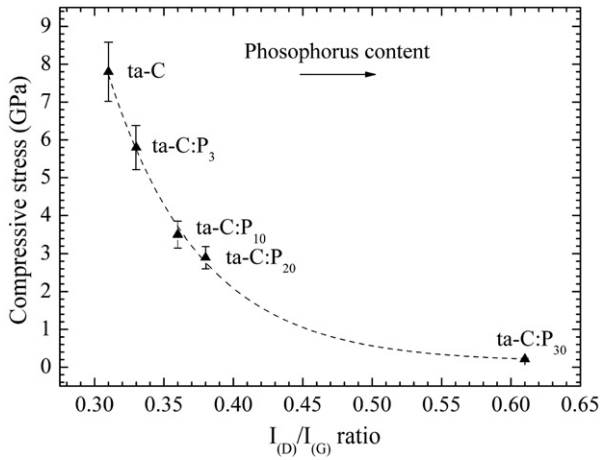

Fig. 3. Variation of the intensity ratio of G and D peaks, $I_{(D)}/I_{(G)}$, versus compressive stress for ta-C and ta-C:P films.

stress. When PH_3 exceeds 20 sccm, $I_{(D)}/I_{(G)}$ ratio represents an abrupt enhancement to 0.61 for ta-C:P_{30}, leading to a 2.7-GPa relief in stress. The relaxation of the stress is interpreted as the reduction of the local distortions in the films and the rearrangement of the atomic bonding structures. When phosphorus atoms are introduced into the carbon network, some sites of carbon are replaced by phosphorus. This process forms a small fraction of new sp^2-bonded carbon without appreciable increase in sp^2 clusters as phosphorus content rises from 0 up to 8.3 at.%. Since one of the hybridized orbits of phosphorus is filled, phosphorus incorporation results in a decreased coordination number in some degree. Consequently, local distortions are released and compressive stress caused by network overconstraining is reduced, as discussed for nitrogen doped a-C films [29]. When phosphorus fraction is as high as 16.8 at.%, sp^2 content increases to a certain high level, implying that phosphorus favors sp^3 sites to sp^2 sites transition. Graphitization can therefore progress around the phosphorus atoms and the olefinic sp^2-bonded carbon in chains cluster into higher-ordered aromatic configurations. The increased size in the carbon rings will substantially enhance the D peak intensity in the Raman spectra, exhibiting a notable "peak shoulder". Due to the shorter bond length of sp^2 sites in the in-plane size, a biaxial compressive stress will be relieved from their σ planes in terms of the transformation of π bonds aligned in the vertical orientation of the planes [30]. In this case, the ordering structures give a satisfying interpretation for pronounced internal stress relief at high content of phosphorus incorporation.

3.3. Conductive behaviors of ta-C:P films

Fig. 4 displays the relationship between the optical gap E_{04} and phosphorus content in the films. It is generally believed that the optical gap in a-C films is determined by the gap between π states and π^* states on sp^2 site [31]. The narrowing in E_{04} from 1.82 eV to 1.31 eV with phosphorus stoichiometry varying from 0 to 6.8 at.% and the increase in the π/π^* electronic states on sp^2 site are related to the enhancement in the sp^2-C contents in ta-C:P films. Progressive saturation of sp^2 sites by excessive H is responsible for the slight increase in E_{04} when PH_3 exceeds 20 sccm, as discussed in Section 3.1.

For further examine whether the efficient doping has taken place, the variation of electrical conductivity σ with temperature for ta-C and ta-C:P films is analyzed, which provides important information on the conduction mechanism of materials. There are usually three conduction mechanisms for amorphous semiconductors, namely the conduction in extended states at higher temperature, the conduction in band tails

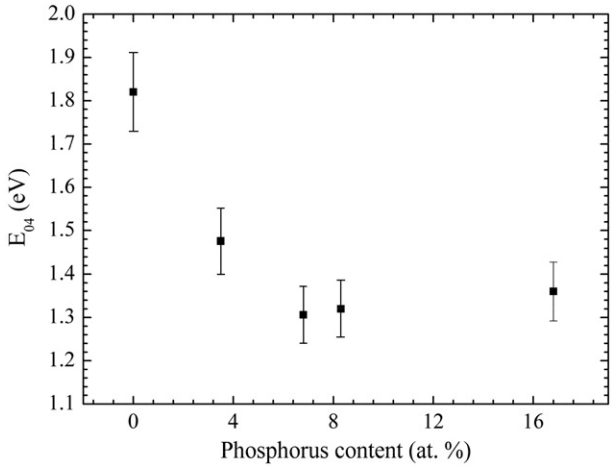

Fig. 4. Relationship between the optical band gap and phosphorus content for ta-C and ta-C:P films.

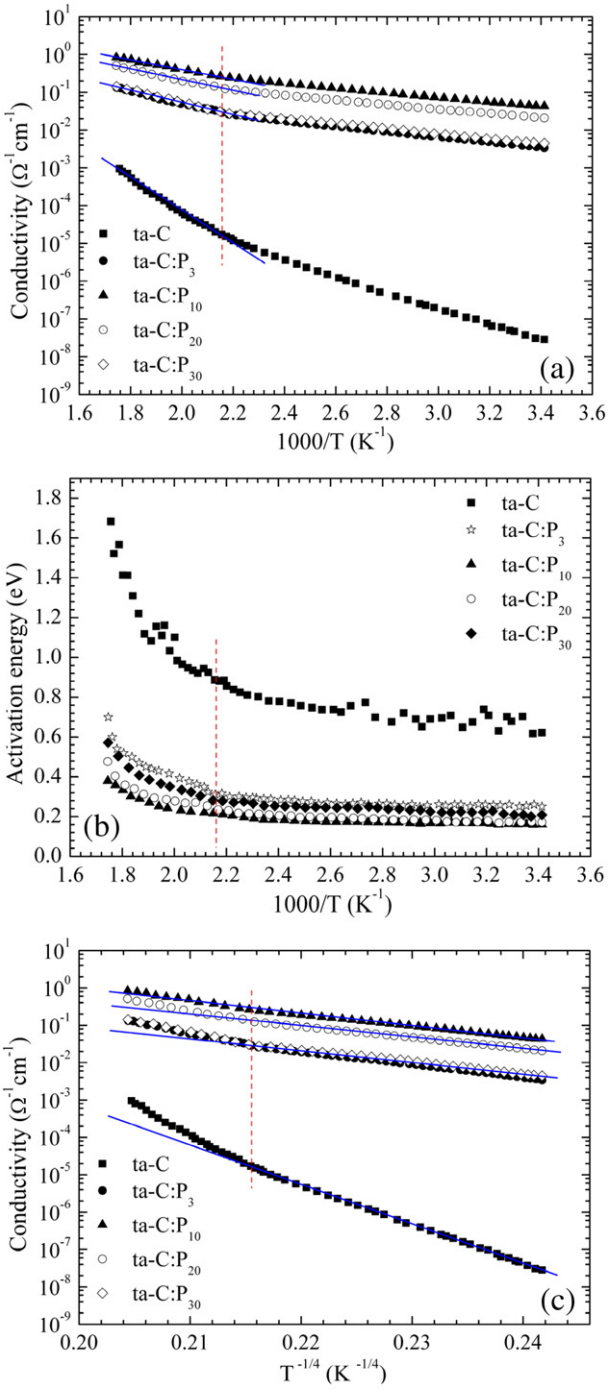

Fig. 5. (a) Arrhenius plots of the electrical conductivity versus the reciprocal temperature for the films synthesized at different PH_3 flow rates. (b) Actual activation energy calculated from Arrhenius curves dependence of reciprocal temperature for the films with different phosphorus contents. The straight lines are guides for the eye. (c) Mott plots of the electrical conductivity as a function of $T^{-1/4}$ for ta-C and ta-C:P films.

states and the conduction in localized states at the Fermi level at lower temperature [32]. For the higher temperature state, the carriers are thermally activated to the extended states, while the variable range hopping (VRH) conduction proposed by Mott is acceptable for the lower temperature case [33]. Fig. 5 (a) illustrates the dependence of the logarithm of the dark conductivity on reciprocal temperature. This does not follow the simple Arrhenius law

$$\sigma(T) = \sigma_0 \exp(-E_{act}/kT) \quad (3)$$

since logσ(T) versus 1/T curves are not linear at the entire range of measurements (293–573 K), where σ_0, E_{act} and k are the pre-exponential constant, activation energy and Boltzmann constant, respectively. This hints that two conduction mechanisms should be considered at different temperature ranges. Furthermore, a strong fluctuation of E_{act} is observed from Fig. 5(b) when the temperature is over 463 K, indicating a change of conduction mechanism. Koos et al. also investigated the thermally activated conduction of a-C films in the extended state in the high-temperature range, found a continuous change of logσ(T) with 1/T and explained this as the broad distribution of band tail states at sp^2 sites [34]. Using the Arrhenius law, the activation energy E_{act} and the prefactor σ_0 at the temperature above 463 K are determined and summarized in Table 3. E_{act} decreases from 0.78 eV for ta-C to 0.24 eV for ta-C:P_{10} and slightly increases to 0.31 eV for ta-C:P_{30} film. An opposite change of σ_0 is observed with increasing phosphorus content (except for ta-C). It is usually suggested that σ_0 is sensitive to the changes in the film microstructures and gives information on conduction mechanisms. The lower σ_0 ($<10\ \Omega^{-1}\ cm^{-1}$) indicates that the conduction is attributed to a hopping transport in localized states, while the higher σ_0 ($>100\ \Omega^{-1}\ cm^{-1}$) hints the thermally activated conduction in extended states [35]. Therefore, the conduction of ta-C:P films at above 463 K is controlled by thermally activated process of carriers. ta-C:P_{10} film with maximal σ_0 represents excellent ability of activated conduction in extended states compared with other ta-C:P films due to the proper sp^2-C and H contents [35]. Fig. 5(a) also validates the corresponding increase in the conductivity of ta-C by several orders of magnitude to a maximum for ta-C:P_{10} film and the final decrease by an order for ta-C:P_{30} film.

If the curves at the temperature below 463 K are also fitted with Eq. (3), the σ_0 values are between 0.5 and 5.4 $\Omega^{-1}\ cm^{-1}$, indicating the hopping conduction in localized states [35]. Moreover, we analyze the conductivity in this temperature range via the log$\sigma(T)$ versus $T^{-1/4}$ curve according to Mott's equation [33]

$$\sigma(T) = \sigma_{00} \exp\left(-(T_0/T)^{1/4}\right), \tag{4}$$

where the perfactor σ_{00} and the slope $T_0^{1/4}$ are related to the distribution of localized electronic states. An excellent linear fit is obtained for all the films (Fig. 5c) and the resulted σ_{00} and $T_0^{1/4}$ are displayed in Table 3. To discriminate the hopping near the Fermi level and the hopping in band tails, the dependent relation of σ_{00} on $T_0^{1/4}$ is shown in Fig. 6. The positive variation of σ_{00} with $T_0^{1/4}$ is in disagreement with Mott's model for VRH but quantitatively agrees with the band tail hopping (BTH) model [36]. This point was confirmed by many previous reports in which the conductive behaviors of a-C materials were examined [35,37,38]. It is suggested that the hopping transport is extremely sensitive to the change in the density of states distribution. A structure transition towards graphitized carbon film can provide large numbers of localized electronic π and π* states. The localization radius therefore decreases with increasing impurity content [39]. π electrons represent more excellent ability of jumping within hopping sites, resulting in a sharp increase in the conductivity of films. However, higher PH_3 magnitude may introduce more H atoms which possibly compensate the hopping sites in ta-C:P structures in some degree and lead to the drop of the electrical conductivity as reported in a-C:N(H) films [40]. Therefore, ta-C:P_{10} film with lower $T_0^{1/4}$ represents a better conductive ability compared with other ta-C:P films [35].

Table 3
Fitting parameters of σ_0, E_{act}, σ_{00} and $T_0^{1/4}$ using Arrhenius and Mott models for ta-C and ta-C:P films prepared at different PH_3 flow rates

Sample	Prefactor σ_0 ($\Omega^{-1}cm^{-1}$)	Activation energy E_{act} (eV)	Prefactor σ_{00} ($\Omega^{-1}\ cm^{-1}$)	Slope $T_0^{1/4}$ ($K^{1/4}$)
ta-C	2.2×10^4	0.78	2.4×10^{17}	238.5
ta-C:P_3	103.9	0.34	6.5×10^5	79.7
ta-C:P_{10}	181.9	0.24	2.8×10^5	66.3
ta-C:P_{20}	148.8	0.28	3.6×10^5	70.0
ta-C:P_{30}	121.8	0.31	4.1×10^5	75.2

The related error for all values is less than 5%.

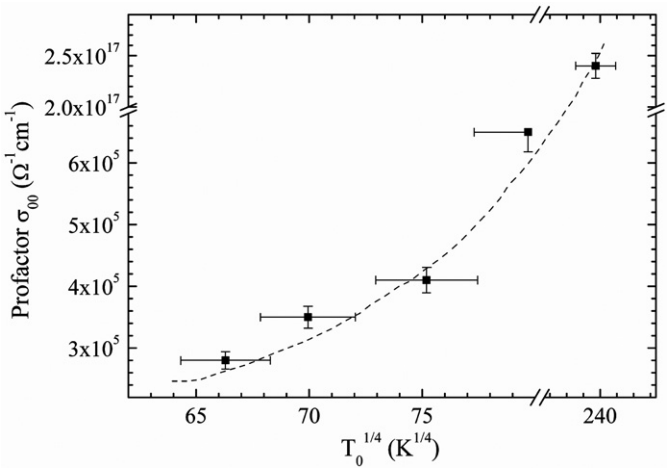

Fig. 6. Variation of the prefactor σ_{00} as a function $T_0^{1/4}$ at the temperature below 463 K for ta-C and ta-C:P films.

The rectifying I–V characteristics of Au/ta-C:P/p-Si/Al structures are plotted as a function of applied voltage, as shown in Fig. 7. When a metal is deposited on the top of a semiconductor, a Schottky contact or an ohmic contact is formed, depending on the doping level of semiconductor, the interface properties, and the difference of work functions between the metal and the semiconductor [41]. As shown in the figure, the Schottky contact is formed between Au and ta-C:P film due to the rectification capability (the forward current is 1–2 orders of magnitude larger than the reverse current for any ta-C:P film). Furthermore, the rectifying nature is also retained after annealing at 400 °C because of the nonreactive interface and the absence of carbides. Two reverse polarities are observed by supplying a negative bias to the structures of ta-C/p-Si and ta-C:P/p-Si, suggesting the n-type conduction nature of ta-C:P films in terms of the p-type one of ta-C. The ratio between the forward and reverse currents at a given voltage for ta-C:P_{10} film is bigger than those of ta-C:P_3 and ta-C:P_{30} films. The pronounced rectifying behavior of ta-C:P_{10} film further indicates its excellent conductive ability at room temperature.

By above analysis we depict the conduction process as follows. When phosphorus is incorporated into the carbon network, sp^2-

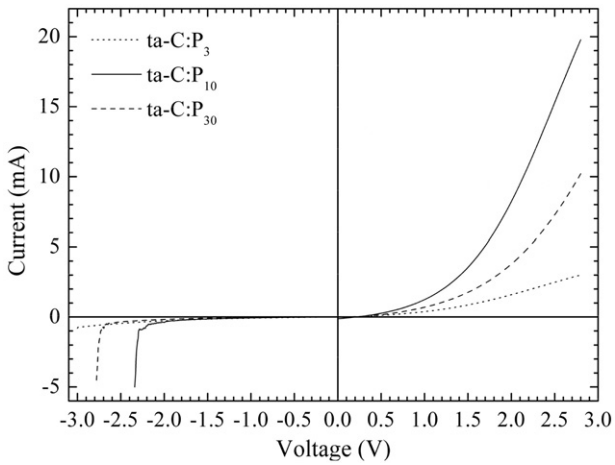

Fig. 7. I–V characteristics of Au/ta-C:P/p-Si/Al structures for ta-C:P films deposited at varying PH_3 flow rates.

bonded C sites increase, accompanied by a significant increase in the density of states near the band edge, a decrease in the localization radius and a narrowing in the optical gap of carbon film. Carriers are easily excited into the localized states at the conduction band edges at the temperature below 463 K and represent relatively high electrical conductivity by the hopping conduction. Therefore, ta-C:P films show an electronic structure with a large number of 'n-type' band tail states. With the further increase of temperature, the carriers are thermally activated to the extended states and ta-C:P films indicate a thermally activated conduction mechanism.

4. Conclusions

Phosphorus incorporated tetrahedral amorphous carbon (ta-C:P) films are prepared using FCVA technique with PH_3 as the dopant. The effect of phosphorus concentration on microstructure, stress and electrical conductivity of ta-C:P films is discussed via the analyses of Raman, IR, intrinsic stress, temperature dependent conductivity and current–voltage curves. It can be inferred that the introduction of up to 20-sccm PH_3 does not substantially alter the dominant amorphous structure of ta-C but plays a modulatory role in the local distortions and the evolution of sp^2 sites. However, the influence of phosphorus impurities on the stress state and electrical properties of ta-C:P films is dramatic. Phosphorus incorporation reduces the structural distortions, releases the overconstraining network and results in a monotonous decrease of intrinsic compressive stress for ta-C film. The temperature dependence of conductivity indicates the thermally activated conduction of carriers in extended states and hopping conduction in localized band tail states near conduction band edges at above and below 463 K, respectively. On the other hand, higher phosphorus impurities induce a large number of sp^2 sites and clustering. This developed ordering-ring configuration releases the biaxial compressive stress owing to the transformation of π bonds. However, excess H atoms may widen the band gap and lengthen the localization radii by saturating some sp^2 sites, leading to a decline of the electrical conductivity. The rectifying nature of ta-C:P heterojunction structures is expected to be predominated by the mechanism of n-type conduction.

Acknowledgments

The authors would like to thank the National Natural Science Foundation of China (Grant No. 50602012) for its financial support and Dr. Sun. Mingren, Chen Yajie, Zhao Guijie and Lv Zhe for their assistance provided in doing XPS, Raman, optical and electrical measurements.

References

[1] D.R. Mckenzie, D. Muller, B.A. Pailthorpe, Phys. Rev. Lett. 67 (1991) 773.
[2] T.A. Friedmann, J.P. Sullivan, J.A. Knapp, D.R. Tallant, D.M. Follstaedt, D.L. Medlin, P.B. Mirkarimi, Appl. Phys. Lett. 71 (1997) 3820.
[3] A.C. Ferrari, B. Kleinsorge, N.A. Morrison, A. Hart, V. Stolojan, J. Robertson, J. Appl. Phys. 85 (1999) 7191.
[4] B.K. Tay, X. Shi, E. Liu, S.P. Lau, L.K. Cheah, Z. Sun, J. Shi, Surf. Coat. Technol. 120–121 (1999) 448.
[5] B.K. Tay, Y.H. Cheng, X.Z. Ding, S.P. Lau, X. Shi, G.F. You, D. Sheeja, Diamond Relat. Mater. 10 (2001) 1082.
[6] O.R. Monteiro, M.P. Delplancke-Ogletree, I.G. Brown, Thin Solid Films 342 (1999) 100.
[7] A.Y. Wang, H.S. Ahn, K.R. Lee, J.P. Ahn, Appl. Phys. Lett. 86 (2005) 111902.
[8] M. Chhowalla, Y. Yin, G.A.J. Amaratunga, D.R. McKenzie, Th. Frauenheim, Appl. Phys. Lett. 69 (1996) 2344.
[9] B. Kleinsorge, A. Ilie, M. Chhowalla, W. Fukarek, W.I. Milne, J. Robertson, Diamond Relat. Mater. 7 (1998) 472.
[10] V.S. Veerasamy, J. Yuan, G.A. Jmaratunga, W.I. Milne, K.W.R. Gilkes, M. Weiler, L.M. Brown, Phys. Rev. B 48 (1993) 17954.
[11] L.K. Cheah, X. Shi, J.R. Shi, E.J. Liu, S.R.P. Silva, J. Non-Cryst. Solids 242 (1998) 40.
[12] H.S. Jung, H.H. Park, Diamond Relat. Mater. 12 (2003) 1373.
[13] V.S. Veerasamy, G.A.J. Amaratunga, C.A. Davis, A.E. Timbs, W.I. Milne, D.R. McKenzie, J. Phys., Condens. Matter 5 (1993) Ll69.
[14] M. Rusop, T. Soga, T. Jimbo, Sol. Energ. Mater. Sol. C 90 (2006) 291.
[15] K.M. Krishna, M. Umeno, Y. Nukaya, T. Soga, T. Jimbo, Appl. Phys. Lett. 77 (2000) 1472.
[16] C.L. Tsai, C.F. Chen, C.L. Lin, J. Appl. Phys. 90 (2001) 4847.
[17] S.C.H. Kwok, J. Wang, P.K. Chu, Diamond Relat. Mater. 14 (2005) 78.
[18] G.M. Fuge, P.W. May, K.N. Rosser, S.R.J. Pearce, M.N.R. Ashfold, Diamond Relat. Mater. 13 (2004) 1442.
[19] A.P. Liu, J.Q. Zhu, J.C. Han, H.P. Wu, W. Gao, Electroanalysis 19 (2007) 1773.
[20] F. Claeyssens, G.M. Fuge, N.L. Allan, P.W. May, M.N.R. Ashfold, Dalton Trans. 19 (2004) 3085.
[21] A.S. Argon, V. Gupta, H.S. Landis, J.A. Cronie, Mater. Sci. Eng. A 107 (1989) 41.
[22] C. Oppedisano, A. Tagliaferro, Appl. Phys. Lett. 75 (1999) 3650.
[23] A.C. Ferrari, S.E. Rodil, J. Robertson, Phys. Rev. B 67 (2003) 155306.
[24] A.C. Ferrari, J. Robertson, Phys. Rev. B 61 (2000) 14095.
[25] J. Robertson, Mater. Sci. Eng. R 37 (2002) 129.
[26] G. Adamopoulos, J. Robertson, N.A. Morrison, C. Godet, J. Appl. Phys. 96 (2004) 6348.
[27] E. Kurita, Y. Tomonaga, S. Matsumoto, K. Ohno, H. Matsuura, J. Mol. Struct., Theochem. 639 (2003) 53.
[28] J. Ristein, R.T. Stief, L. Ley, W. Beyer, J. Appl. Phys. 84 (1998) 3836.
[29] F.L. Freire Jr., D.F. Franceschini, Thin Solid Films 293 (1997) 236.
[30] A.C. Ferrari, S.E. Rodil, J. Robertson, W.I. Milne, Diamond Relat. Mater. 11 (2002) 994.
[31] J. Robertson, Philos. Mag., B 76 (1997) 335.
[32] X. Shi, H. Fu, J.R. Shi, L.K. Cheah, B.K. Tay, P. Hui, J. Phys., Condens. Matter 10 (1998) 9293.
[33] N.F. Mott, Philos. Mag. 19 (1969) 835.
[34] M. Koos, S.H.S. Moustafa, E. Szilagyi, I. Pocsik, Diamond Relat. Mater. 8 (1999) 1919.
[35] G. Lazar, K. Zellama, M. Clin, C. Godet, Appl. Phys. Lett. 85 (2004) 6176.
[36] C. Godet, Diamond Relat. Mater. 12 (2003) 159.
[37] J.J. Hauser, J.R. Patel, Solid State Commun. 18 (1976) 789.
[38] K. Rohwer, P. Hammer, J.U. Thiele, J. Non-Cryst. Solids 137–138 (1991) 843.
[39] S. Kumar, C. Godet, A. Goudovskikh, J.P. Kleider, G. Adamopoulos, V. Chu, J. Non-Cryst. Solids 338–340 (2004) 349.
[40] W.L. Zhang, Y.B. Xia, J.H. Ju, L.J. Wang, Z.J. Fang, M.L. Zhang, Solid State Commun. 126 (2003) 163.
[41] J.L. Freeouf, J.M. Woodall, Appl. Phys. Lett. 39 (1981) 727.